Predefined angle of attack and corner shape effects on the effectiveness of square-shaped galloping energy harvesters

Mingjie Zhang[1], Abdessattar Abdelkefi[2], Haiyan Yu[3], Xuyong Ying[4], Oleg Gaidai[5], Junlei Wang[6,*]

1. Department of Structural Engineering, Norwegian University of Science and Technology, Trondheim, 7491, Norway.

2. Department of Mechanical and Aerospace Engineering, New Mexico State University, Las Cruces, NM 88003, USA.

3. School of Civil and Environmental Engineering, Harbin Institute of Technology, Shenzhen, 518055, China.

4. Jiangsu Transportation Institute Co. Ltd., Nanjing, 211112, China

5. Jiangsu University of Science and Technology, School of Naval Architecture and Offshore Engineering, Zhenjiang, China.

6. School of Mechanical and Power Engineering, Zhengzhou University, Zhengzhou 450000, China.

*Corresponding author: Junlei Wang, Email address: jlwang@zzu.edu.cn

Abstract

Energy harvesting based on transverse galloping of a square cylinder has been widely studied while the effects of angle of attack and corner shape remain unclear. This study proposes to explore the impacts of these two parameters on the characteristics and effectiveness of square-based galloping energy harvesting systems using a coupled fluid-structure-electrical model. It is demonstrated that the onset speed of instability is dependent on the electrical load resistance. Additionally, the load resistance value corresponding to the maximum onset speed of galloping is inversely proportional to the natural frequency of the energy harvester. Further, the onset wind speed of instability and the dynamic response of the energy harvester are largely affected by the angle of attack and corner shape. The rounded corners make the onset velocity less sensitive to the angle of attack. The considered square cylinders with different corner shapes exhibit the largest transverse displacements at the angle of attack $\alpha_0 = 0°$, while the displacements at $\alpha_0 = 2°$ are only slightly lower than those at $\alpha_0 = 0°$. In general, the rounded corners slightly decrease the displacements and power outputs of the harvester. However, the rounded corners enhance the robustness of the harvester by making its performance less sensitive to the angle of attack within $\alpha_0 = 0° \sim 6°$. It is also shown that the type of instability is strongly dependent on the angle of attack and corner shape which may result in the presence of unexpected bifurcations, such as the subcritical and saddle-node ones.

Keywords: Piezoelectric energy harvesting; transverse galloping; square cylinder; predefined angle of attack; corner shape

1. Introduction

Harvesting energy from mechanical vibrations is a promising technology for powering low-energy consumption devices including health monitoring and wireless sensor networks, actuators, and micro-electromechanical systems [1, 2], etc. Energy harvesting from ambient vibrations has been largely investigated with considerable efforts conducted to broaden the effective bandwidth of harvesting energy from various vibration sources [3-5]. The following principles are often employed to harvest energy, e.g. piezoelectric [6], electromagnetic [7], triboelectric [8], and their combinations [9]. As a ubiquitous natural phenomenon, wind has already been working as a significant renewable energy resource [10, 11]. Thus, energy extraction based on wind-induced vibrations has raised considerable research attention [12-14].

Energy can be harvested from wind-induced vibrations through one of three well-known vibration mechanisms, i.e., vortex-induced vibrations [15-19], galloping [20-23], and flutter [24-26] although other vibration mechanisms also exist [27]. The transverse galloping of a bluff body, e.g., a square cylinder, has been widely studied as an energy harvester since it is effective once the onset wind velocity for galloping is achieved. Transverse galloping was first studied systematically by Den Hartog [28], who demonstrated that the onset velocity of galloping instability can be obtained using the quasi-steady aerodynamic theory. Parkinson and co-authors [29, 30] showed that the vibration amplitude of transverse galloping can be well predicted by the quasi-steady theory. Since then, the galloping of different structures, e.g., towers and power transmission lines, has been well studied. Barrero-Gil et al. [31] firstly demonstrated the possibility of harvesting energy from transverse galloping. They further carried out several theoretical studies on the performances of galloping-based energy harvesters using a reduced-order model with the quasi-steady aerodynamic theory. Abdelkefi and co-authors [12, 20, 32-35] highlighted experimentally and numerically the influences on the effectivenesses of galloping energy harvesters of the tip body shape, the flow features (e.g., the Reynolds number), the accuracy of the aerodynamic force coefficients, and the inclined angle of the tip body relative to wind flow. Yang et al. [22] presented wind tunnel experiments to study the effectiveness of energy harvesters with several different cross-sections (e.g., square, rectangular, and triangular) as galloping bluff bodies. A comparison of these energy harvesters suggested that the one with a bluff body of square configuration has the greatest efficiency. Zhang et al. [36] conducted numerical simulations to study the effects of damping and mass properties on the effectiveness of a galloping energy harvester with a square bluff body. Based on wind tunnel experiments and numerical simulations, Wang et al. [17] designed a bluff body (composed of a half circular section and a half square section) for galloping-based energy harvesting. They showed that, compared with a suqare cylinder, their design can immensely reduce the threshold flow velocity for the occurrence of large vibrations and hence

beneficial for the output voltage.

Despite extensive existing investigations in terms of galloping energy harvesters with square cylinder bluff bodies, the square cylinders are placed at a 0° angle of attack relative to the oncoming wind flow in almost all these studies. The influences of the predefined wind angle of attack on the effectiveness of a galloping-based energy harvester with a square cylinder bluff body remain unclear. Therefore, the robustness of the considered energy harvester with changing the angle of attack is unknown. Indeed, the angle of attack of an operating energy harvester varies with the oncoming flow direction, and hence it is necessary to evaluate the effectiveness of an energy harvester within a range of angles of attack. As is well known, the vibration mechanism (i.e., galloping, vortex-induced vibration, or combination of two mechanisms) of a square cylinder is dependent on the predefined wind angle of attack, mass ratio, and damping ratio. For a low-mass square cylinder (i.e., $m^* = 2.2$), Nemes et al. [37] and Zhao et al. [38] experimentally demonstrated that this prismatic cylindrical structure performed galloping instabilities for angles of attack 0° ~ 10°, while it exhibited vortex-induced vibrations in the range of 15° ~ 45°. Tang and Zhou [39] demonstrated that the effect of the predefined wind angle of attack on the mechanisms of a square cylinder is dependent on its mass ratio and spring stiffness. Zhang et al. [40] investigated the galloping vibrations of a rectangular cylinder at varying predefined angles of attack with the quasi-steady aerodynamic theory. They showed that the angle of attack affected both the onset wind speed for galloping instability and the vibratory amplitudes after the onset wind speed.

The wind-induced vibration of a square cylinder (and hence the performance of a square-shaped galloping energy harvester) may be also largely influenced by its corner shape. Optimization of the corner shape may improve the efficiency or robustness of an energy harvester. Several optimal designs of corner shapes have been designed aiming at modifying the galloping response of a square bluff body [41]. Carassale et al. [42] showed that the aerodynamics of a square cylinder can be affected largely by changing its sharp corners into rounded ones. More specifically, the rounded corners resulted in a remarkable reduction of the onset galloping velocity at non-zero predefined angles of attack, which might be a beneficial feature for energy harvesting.

The present paper investigates numerically the influences of the predefined wind angle of attack and the corner shape on the piezoelectric energy harvesting based on the transverse galloping of a square cylinder. A coupled fluid-structure-electrical model is developed to represent the system being analyzed, in which the aerodynamic part is approximated by the quasi-steady theory. Three bluff body configurations are considered, i.e., an ideal square cylinder with sharp-edge corners and two modified square cylinders with different rounded corner radii. The aerodynamic coefficients of these configurations originate from the experiments of Carassale et al. [42]. The effectivenesses of the considered energy harvester are analyzed for different angles of attack

and corner shapes. The rest of this study is organized into few sections. In section 2, the representative piezoaeroelastic model is derived with a particular focus on the impacts of the corner shape and angle of attack on the aerodynamic force representation. A discussion on the limits of applicability of the quasi-steady assumption for the galloping force and the piezoaeroelastic model verification is performed. After that, an exploration of the effects of the angle of attack and the corner shape on the onset velocity for galloping instability of the coupled system is examined and discussed in section 3. Then, in section 4, the bifurcation diagrams and performance of the piezoaeroelastic energy harvester under consideration are determined with focusing on the influences of the predefined angle of attack and corner shape on the displacement and harvested power. Section 5 concludes the most important results of this investigation.

2. Representative model for galloping systems with predefined angle of attack and corner shapes

As schematically shown in Figure 1(a), a typical galloping-based piezoelectric energy harvester includes a square cylinder as a tip body that is subjected to a wind speed U, and a cantilever beam bonded with a piezoelectric transducer. Figure 1(b) defines the predefined wind angle of attack α_0, i.e., the angle between the wind flow and the chord line of the tip body. The rounded corner shape is quantified by the radius r of the corner, as illustrated in Figure 1(c), in which d is the width of the square cylinder.

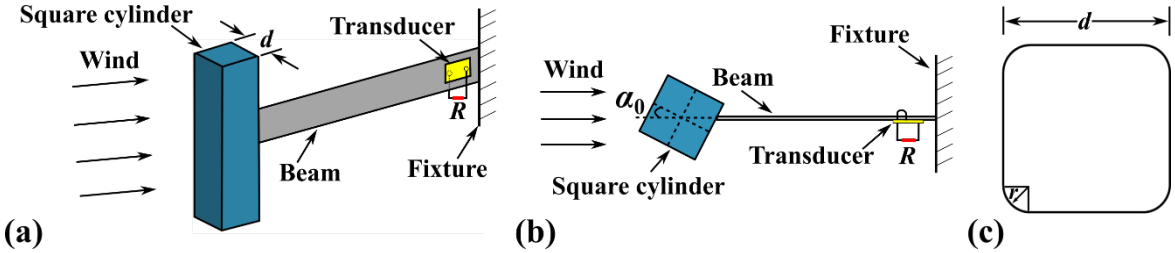

Figure 1. Galloping-based energy harvester: (a) schematic of energy harvester, (b) definition of angle of attack, and (c) definition of corner radius.

The aerodynamic load on the tip body may lead to the oscillation of the cantilever beam and hence an electrical energy production at the piezoelectric transducer. According to the quasi-steady theory [29, 30], the aerodynamic load acting on the square cylinder can be approximated as:

$$F_x = 0.5\rho U^2 d C_{Fx} = 0.5\rho U^2 d \sum_{j=1}^{J} A_j \left(\alpha_0 + \frac{\dot{x}}{U}\right)^j \tag{1}$$

where C_{Fx} represents the aerodynamic lift force coefficient, ρ is the density of the fluid, A_j ($j = 1 \sim J$) are aerodynamic damping coefficients (which should be calculated based on a polynomial fitting of the $C_{Fx}(\alpha)$ data). Additionally, x denotes the displacement and the overdot indicates the derivative relative to time t.

In the quasi-steady aerodynamic theory, it is assumed that the time length required for the wind flow to travel over the structure and convert enough distance downstream is much smaller than the one of the structural oscillation. Hence, the accuracy of the theory is guaranteed only for cylinders with relatively high onset wind speeds of instability, that is, its accuracy in terms of simulating the galloping increases with increasing the mass-damping parameter (often represented by the Scruton number, $Sc = 4\pi m\xi_n/\rho d^2$) of the cylinder [43].

The $C_{Fx}(\alpha)$ curves for ideal square cross-sections with sharp-edge corners were experimentally measured by several authors (e.g., Parkinson and Smith [29], Laneville [44], and Carassale et al. [42]), as presented in Figure 2. The results of Parkinson and Smith [29] and Carassale et al. [42] were measured in smooth flows with Reynolds numbers around 22,300 and 37,000, respectively, while the results of Laneville [44] were obtained in a turbulent flow field with an intensity of around 6.7% and Reynolds number around 33,000. Clearly, it can be noted from the presented data in Figure 2 that the linear and nonlinear galloping force coefficients of a sharp-edged square cylinder are insensitive to the Reynolds number but remarkably dependent on the turbulence intensity. This observation indicates the significance of accurately determining the environmental conditions where the energy harvester will be implemented. Indeed, the linear coefficient of this aerodynamic force will directly affect the onset speed of galloping instability and hence changes the self-excited motion occurrence and the harvesting capabilities of the galloping-based energy harvester. As for the nonlinear coefficients of the galloping force, they have direct impact on the type of instability (e.g., supercritical or subcritical) with possible presence of the saddle node bifurcation. All these kinds of instabilities will be deeply discussed later.

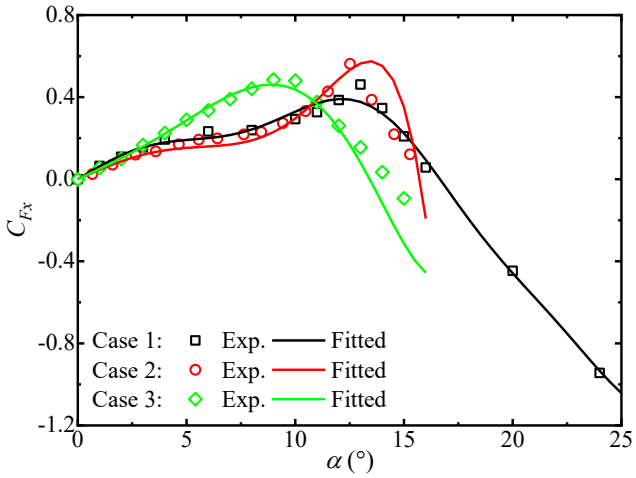

Figure 2. Experimental and fitted aerodynamic coefficients as functions of angle of attack for square cylinders with sharp-edge corners (Case 1 from [42], Case 2 from [29], Case 3 from [44]).

The plotted curves in Figure 3 presents the variations of the galloping force coefficient, $C_{Fx}(\alpha)$, for the square cylinders with different rounded corner radii, i.e., r/d = 0, 1/15, and 2/15, as experimentally measured

by [42]. Polynomial representations of these aerodynamic coefficients are listed in Table 1. The coefficients for Case 1 and two round-edge cylinders are fitted as 19th-order polynomials, while those for Cases 2 and 3 adopt the fittings in [29] and [45], respectively. The roles of the angle of attack and corner shapes on the aerodynamic coefficients (and hence galloping responses) are clearly highlighted in the plots shown in Figure 3. By further inspecting Figure 3, it is clear that both the linear and nonlinear characteristics of the galloping are affected by the shape corner of the cylindrical structure. In fact, high values of the galloping force coefficient takes place at smaller angles of attack when the rounded corner radius becomes more important. This may result in a change of the nonlinear coefficients of the galloping force representation and hence the changes in the type of instability and system's response. In a quantitative observation of the coefficients shown in Table 1, it is clear that the linear coefficient of the galloping force is the same for $r/d = 0$ and $r/d = 2/15$ and hence it is expected that the onset speed of galloping will not be affected for these two cases when the angle of attack is zero. On the other hand, the linear coefficient of the corner shape of $r/d = 1/15$ is higher than the other two, and consequently, lower values of the onset speed of instability should take place for this case compared to $r/d = 0$ and $r/d = 2/15$ configurations when the angle of attack is zero.

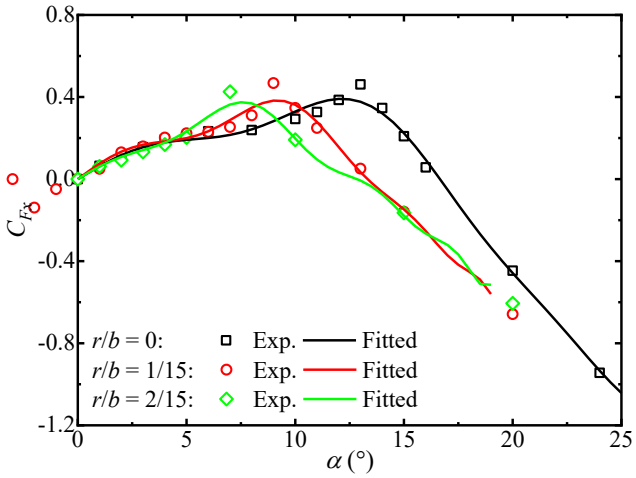

Figure 3. Experimental and fitted aerodynamic coefficients as functions of angle of attack for square cylinders with different rounded corner radii (experimental data from [42]).

Table 1. Polynomial representation of the galloping force.

	A_1	A_3	A_5	A_7	A_9	A_{11}	A_{13}	A_{15}	A_{17}	A_{19}
Case 1 ($r/d = 0$)	3.68	−3.02e2	1.70e4	−4.44e5	6.11e6	−4.93e7	2.42e8	−7.15e8	1.17e9	−8.07e8
Case 2	2.69	−1.68e2	6.27e4	−5.99e5	0	0	0	0	0	0
Case 3	2.83	9.08e1	−4.25e4	3.01e5	0	0	0	0	0	0
$r/d = 1/15$	4.51	−6.26e2	6.08e4	−2.57e6	5.04e7	−3.84e8	−1.76e9	5.28e10	−3.50e11	7.99e11
$r/d = 2/15$	3.68	−5.98e2	1.08e5	−8.12e6	3.08e8	−6.69e9	8.67e10	−6.65e11	2.79e12	−4.91e12

After presenting the galloping force using the quasi-steady approximation and determining the influence of the corner shape and angle of attack on its linear and nonlinear coefficients, a representative reduced-order model for the piezoaeroelastic energy harvesting system can be expressed as [33, 46]:

$$m[\ddot{x}(t) + 2\omega_n\xi_n\dot{x}(t) + \omega_n^2 x(t)] + \theta V(t) = F_x(t) \tag{2a}$$

$$C_p\dot{V}(t) + \frac{V(t)}{R} - \theta\dot{x}(t) = 0 \tag{2b}$$

where the mechanical parameters include the equivalent mass per unit length m, the natural frequency ω_n, and the damping ratio ξ_n; the electrical parameters include the capacitance of the piezoelectric layer C_p, the electrical load resistance R, and the electromechanical coupling coefficient θ; the aerodynamic force is represented by F_x; V is generated voltage to be calculated.

The nonlinear reduced-order model presented in equations (2a) and (2b) for the galloping-based aeroelastic energy harvesting system has been verified by several authors, e.g., [45, 47]. Following these comparative studies between the developed model and the experimental results, it can be concluded that this model can evaluate the response of the galloping-based energy harvesting systems with various predefined angles of attack and corner shapes that are considered in this investigation. It should be stated that the aerodynamic coefficients (and hence galloping behavior) of a cylindrical structure may be affected by several other parameters, e.g., the Reynolds number, the surface roughness, and the turbulent intensity. The aerodynamic coefficients of [42] were measured for cylinders without extra surface roughness in smooth flows. The effect of Reynolds number is insignificant for a sharp-edge cylinder, while the effect may be remarkable for a round-edge cylinder. The effects of these parameters are not further investigated since they are not the main focus of this study.

3. Effects of predefined angle of attack and corner shape on the onset galloping

Next, the influences of the predefined wind angle of attack and corner shape on the effectiveness of galloping-based energy harvesting systems are explored and discussed. To this end, three bluff body configurations are analysed in this study, i.e., an ideal square cylinder with sharp-edge corners and two modified square cylinders with rounded corner radii r/d = 1/15 and 2/15, respectively. Following [46], the mechanical and electrical parameters used in the numerical simulations are m = 440 g/m, ξ_n = 0.0013, d = 1.5 cm, θ = 1.55 mN/V, and C_p = 120 nF.

The effects of the angle of attack, the corner shape, and the electrical load resistance on the onset wind speed for galloping instability are evaluated based on a linear analysis of the fluid-structure-electrical system. To this end, some state variables are firstly introduced as following:

$$\mathbf{Z} = \begin{bmatrix} Z_1 \\ Z_2 \\ Z_3 \end{bmatrix} = \begin{bmatrix} X \\ X' \\ I \end{bmatrix} \tag{3}$$

For a specific initial angle of attack α_0, the equations of motion, that is, equation (2), is expressed as follows:

$$\mathbf{Z}' = \mathbf{AZ} + \mathbf{NLT} \tag{4}$$

where **A** is a matrix having all linear properties of the galloping-based energy harvesting system and NLT represents the nonlinear terms of the system's equations of motion.

It follows from equation (4) that three eigenvalues ($\lambda_j, j = 1 \sim 3$) of matrix **A** can take place for this model. Two of those eigenvalues are complex-conjugate and one of them is always negative due to the presence of the piezoelectric equation. The first two eigenvalues should describe the oscillatory motion of the energy harvesting system. Indeed, when the real part of these eigenvalues changes sign from negative to positive, the onset of instability takes place and hence self-excited motion becomes present. To this end, studying the effects of the corner shape, predefined angle of attack, and electrical load resistance on the stability of the galloping-based energy harvester are analysed by solving the eigenvalues of the system for various flow speeds.

Figure 4 presents the influence of the electrical load resistance on the onset galloping velocity for the energy harvester with the r/d = 1/15 cylinder at a 0° predefined wind angle of attack. The natural frequency of the energy harvester is assumed as $f_n = \omega_n/2\pi$ = 5, 10, 15, 20, 30, or 40 Hz. The onset galloping velocity for a pure aeroelastic system (i.e., a fluid-structure system without piezoelectric coupling effect) is known to depend on the mass ratio, damping ratio, and A_1, i.e., $U_r = 4m^*\xi_n/A_1$. For a system with a very low or very high load resistance, e.g., $R < 10^3$ Ω or $R > 10^7$ Ω, the onset velocity is almost identical to that of a pure fluid-structure system since the influence of piezoelectric coupling is weak. As observed from Figure 4, the onset galloping velocity varies insignificantly with load resistance when the resistance is very low or very high. The variation rate becomes larger in the medium range of load resistance, and a peak value of the onset velocity is achieved within $R = 5\times10^4 \sim 5\times10^5$ Ω depending on the natural frequency. Finally, the onset velocity depends insignificantly on load resistance for a harvester with a higher natural frequency because the shunt damping effect reduces when the natural frequency is increased. It should be mentioned that an increase of the natural frequency is accompanied by a decrease of the electrical load resistance at which the onset speed of galloping instability is maximum. This is expected because the optimal value of the load resistance for maximum global damping is inversely proportional to the natural frequency and capacitance of the energy harvester.

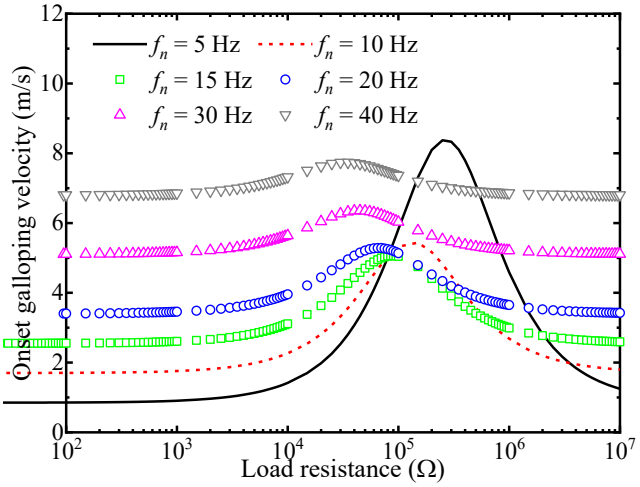

Figure 4. Variation of onset velocity for galloping instability versus electrical load resistance for energy harvester with r/d = 1/15 cylinder at 0° angle of attack.

Figure 5 presents the variation of the onset wind velocity for galloping instability versus angle of attack for energy harvesters with three different bluff body configurations. The natural frequency considered here is f_n =10 Hz. Four electrical load resistances are considered, namely, R = 10^4, 10^5, 10^6, and 10^7 Ω. For each bluff body configuration, the onset velocity for galloping instability first increases with the increase of wind angle of attack and then decreases to a value close to that at α_0 = 0°. This global trend is similar to that observed for a pure aeroelastic system [42]. In a range of small angles of attack (α_0 = 0° ~ 2°), the onset velocities of the three configurations are very close. The linear analysis suggests that the energy harvester with the sharp-edge square cylinder is effective around α_0 = 0° ~ 2° and 8° ~ 10° while less effective around α_0 = 3° ~ 7° due to the higher onset galloping velocity. It is important to note that the rounded corners make the onset velocity less sensitive to the angle of attack. The effective α_0 range of the harvester is also changed by the corner shapes. For the three configurations, the slopes of the $C_{Fx}(\alpha)$ curves become negative, and hence no galloping vibration occurs for α_0 > 10°, 8°, and 6°, respectively.

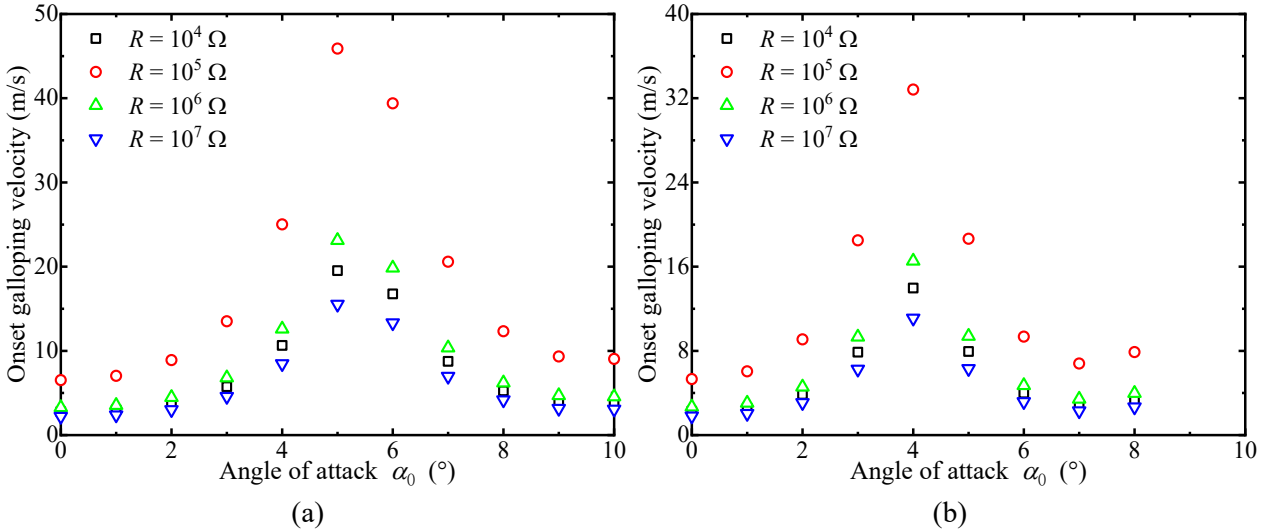

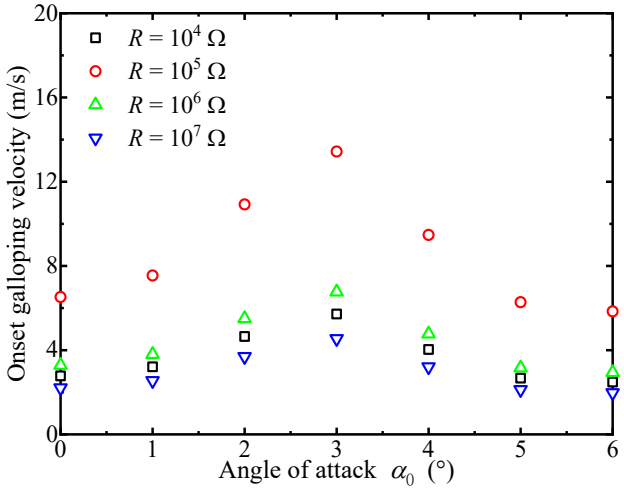

(c)

Figure 5. Variation of onset velocity for galloping instability versus angle of attack for harvesters with (a) sharp-edge cylinder, (b) r/d = 1/15 cylinder, and (c) r/d = 2/15 cylinder.

The onset galloping velocities for energy harvesters with a load resistance of $R = 10^6\ \Omega$ are listed in Table 2. For small angles of attack ($\alpha_0 = 0° \sim 2°$), the onset galloping velocity varies insignificantly with the corner shape. This is expected since the slopes of the $C_{Fx}(\alpha)$ curves are close for the considered cylinders within this range of angles of attack, as shown in Figure 3. The range of α_0 within which the cylinder is able to gallop shrinks with increasing r/d. The rounded corner also makes the onset velocity less sensitive to the angle of attack within $\alpha_0 = 0° \sim 6°$.

Table 2. Onset galloping velocities (m/s) for energy harvesters with load resistance $R = 10^6\ \Omega$.

α_0 (°)	sharp-edge cylinder	r/d = 1/15 cylinder	r/d = 2/15 cylinder
0	3.29	2.68	3.29
1	3.55	3.05	3.80
2	4.48	4.58	5.50
3	6.81	9.32	6.77
4	12.61	16.54	4.77
5	23.13	9.40	3.16
6	19.85	4.71	2.94
7	10.37	3.43	stable
8	6.21	3.97	stable
9	4.70	stable	stable
10	4.56	stable	stable

4. Impacts of the predefined angle of attack and corner shape on the harvester's performance

The nonlinear feature of the fluid-structure-electrical system is further analyzed in this section to study the impacts of the predefined angle of attack and the corner shape on the vibrational response and energy-generating of the present energy harvester. The mechanical and electrical parameters are m = 440 g/m, ζ_n = 0.0013, f_n =10 Hz, d = 1.5 cm, θ = 1.55 mN/V, and C_p = 120 nF. The equations of motion of the system are integrated in the time-domain using the standard Newmark-β algorithm. During the simulation, the wind speed is initiated from 0 m/s and increased to 10 m/s with a 0.1 m/s step. Hence, the simulations are conducted within

0 to 10 m/s. The initial displacement, initial velocity, and initial voltage at the first analyzed wind speed (i.e. 0 m/s) are set as 0.01d, 0, and 0, respectively. To simulate the continuously increasing wind speed that is often conducted in a wind tunnel experiment, the initial displacement for any other wind speed is determined as the steady-state vibration amplitude of the formerly analysed speed while the initial velocity and initial voltage are 0. It is found that a normalized time step of $\Delta\tau = 1/100$ is refined enough to ensure the simulation accuracy. The system response at each wind speed should be simulated for a sufficiently long duration so that the steady-state response is achieved. It should be noted that the bifurcation behavior of the energy harvester may be different if the simulation is performed by increasing or decreasing the oncoming flow velocity. For example, a supercritical Hopf bifurcation occurs at the onset speed of instability. In this case, a smooth increase in the oscillatory amplitude takes place and the increasing/decreasing of the flow speed does not change the bifurcation diagram of the system under investigation. On the other hand, if the increasing/decreasing of the flow speed results in the presence of hysteresis region or an increase in the flow speed leads to a sudden jump at the onset of instability, a subcritical Hopf bifurcation takes place. A saddle-node bifurcation may also occur. In fact, in this case, a supercritical instability with a smooth transition takes place at the onset speed of galloping and then a subcritical jump exists. Details of the bifurcation behaviors can be found in [35].

The bifurcation diagrams plots shown in Figures 6-8 present the effects of angle of attack and electrical load resistance on the transverse displacement of the energy harvesters with three bluff body configurations. As seen from the figures, both the onset velocity for instability and the increasing rate of the bifurcation curve may be affected by the angle of attack. All three cylinders exhibit the largest transverse displacements at the angle of attack $\alpha_0 = 0°$, while the displacements at $\alpha_0 = 2°$ are only slightly lower than those at $\alpha_0 = 0°$. For the sharp-edge cylinder with $R = 10^4$, 10^5, and 10^6, no galloping vibration occurs at $\alpha_0 = 4°$ and 6° within the considered flow velocity range. This is expected from the linear analysis because the onset galloping velocities for these angles of attack are much higher than 10 m/s, as shown in Figure 5. Galloping vibrations are again observed at $\alpha_0 = 8°$ and 10°. Although the onset velocities at $\alpha_0 = 2°$ and 10° are almost consistent, the cylinder has very different galloping responses at these two angles of attack. Furthermore, it is noted that the transverse displacements are considerably smaller for the medium values of load resistance, i.e., around $R = 10^5$ Ω.

A comparison of Figures 6-8 suggests that the galloping response is largely affected by the corner shape. For the cylinder with $r/d = 1/15$, no galloping vibration occurs at $\alpha_0 = 4°$ within the considered flow velocity range. This is also expected from the linear analysis in section 3 since the onset galloping velocity for this angle of attack is much higher than 10 m/s. For the cylinder with $r/d = 2/15$, galloping vibrations are observed for all angles of attack within $\alpha_0 = 0° \sim 6°$. Therefore, the effective α_0 range is expected to be larger for an

energy harvester with a round-edge cylinder if the cylinder is originally placed at a 0° angle of attack (as is usually done in previous studies). It is also noted that the rounded corners slightly decrease the transverse displacements of the energy harvesters.

Inspecting the bifurcation diagrams in Figures 6-8, it is clear that the predefined angle of attack may change the instability of the energy harvester. Indeed, for the sharp edge square cylinder, a saddle-node bifurcation (not shown in the figures since only the responses of the increasing velocity simulation are presented) with the presence of a subcritical jump takes place when $\alpha_0 = 0°$ and 2° and disappears when the predefined angle of attack is increased to higher values ($\alpha_0 = 8°$ and $\alpha_0 = 10°$), after which a supercritical Hopf bifurcation occurs at the onset velocity, as shown in Figures 6(a), (b), and (d). Some specific scenarios of the predefined angle of attack and corner shape results in the presence of the subcritical Hopf bifurcation, such as the case when $\alpha_0 = 4°$ for the sharp edge square cylinder and $\alpha_0 = 2°$ for the energy harvester with $r/d = 2/15$ cylinder, as depicted in Figure 6(d) and Figures 8(a-d), respectively. This means that the predefined angle of attack and corner shape strongly affect the onset speed of galloping instability and the type of instability of the system.

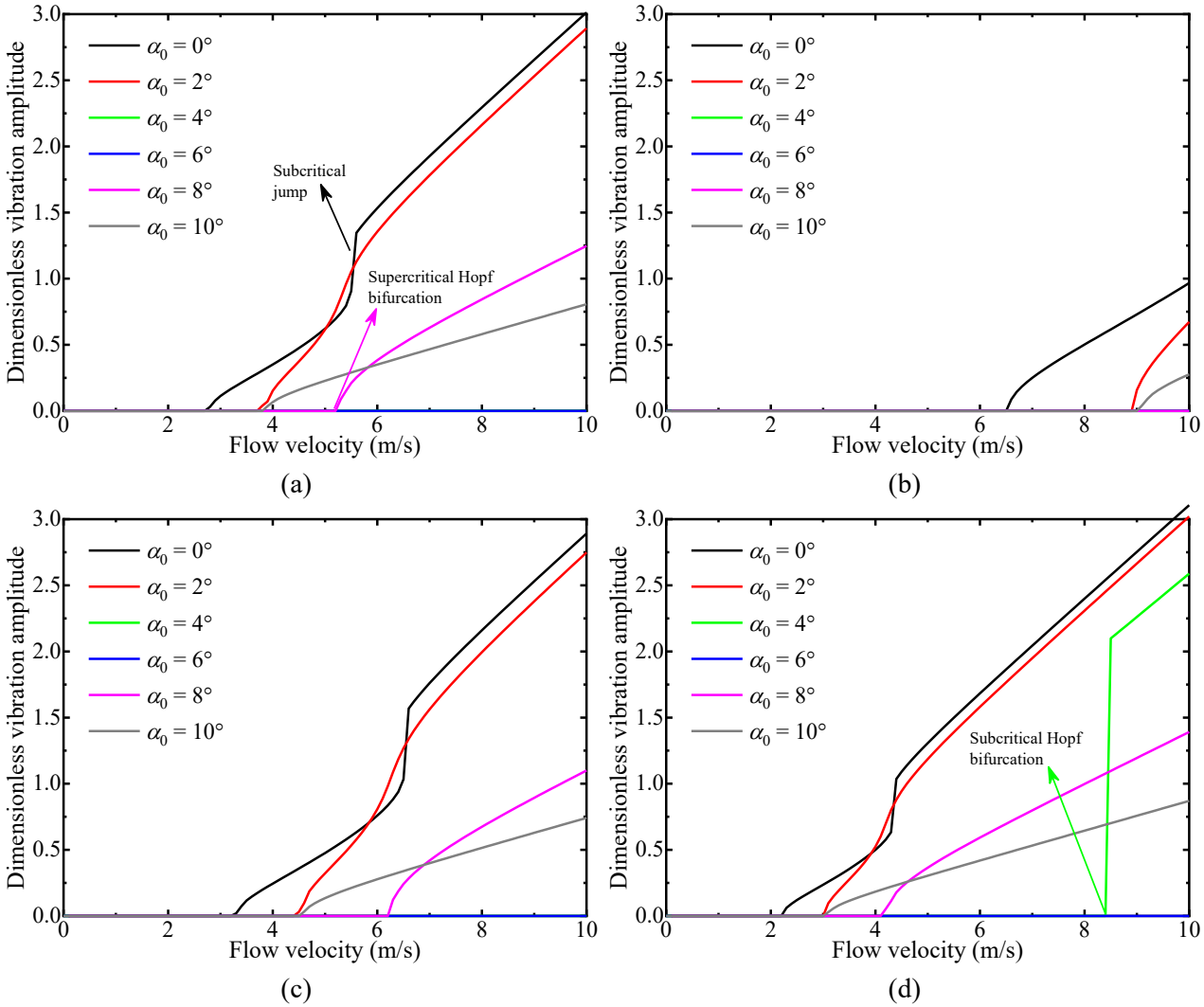

Figure 6. Displacement bifurcation diagrams for energy harvester with sharp-edge cylinder at various

predefined angles of attack and load resistances: (a) $R = 10^4$ Ω, (b) $R = 10^5$ Ω, (c) $R = 10^6$ Ω, and (d) $R = 10^7$ Ω.

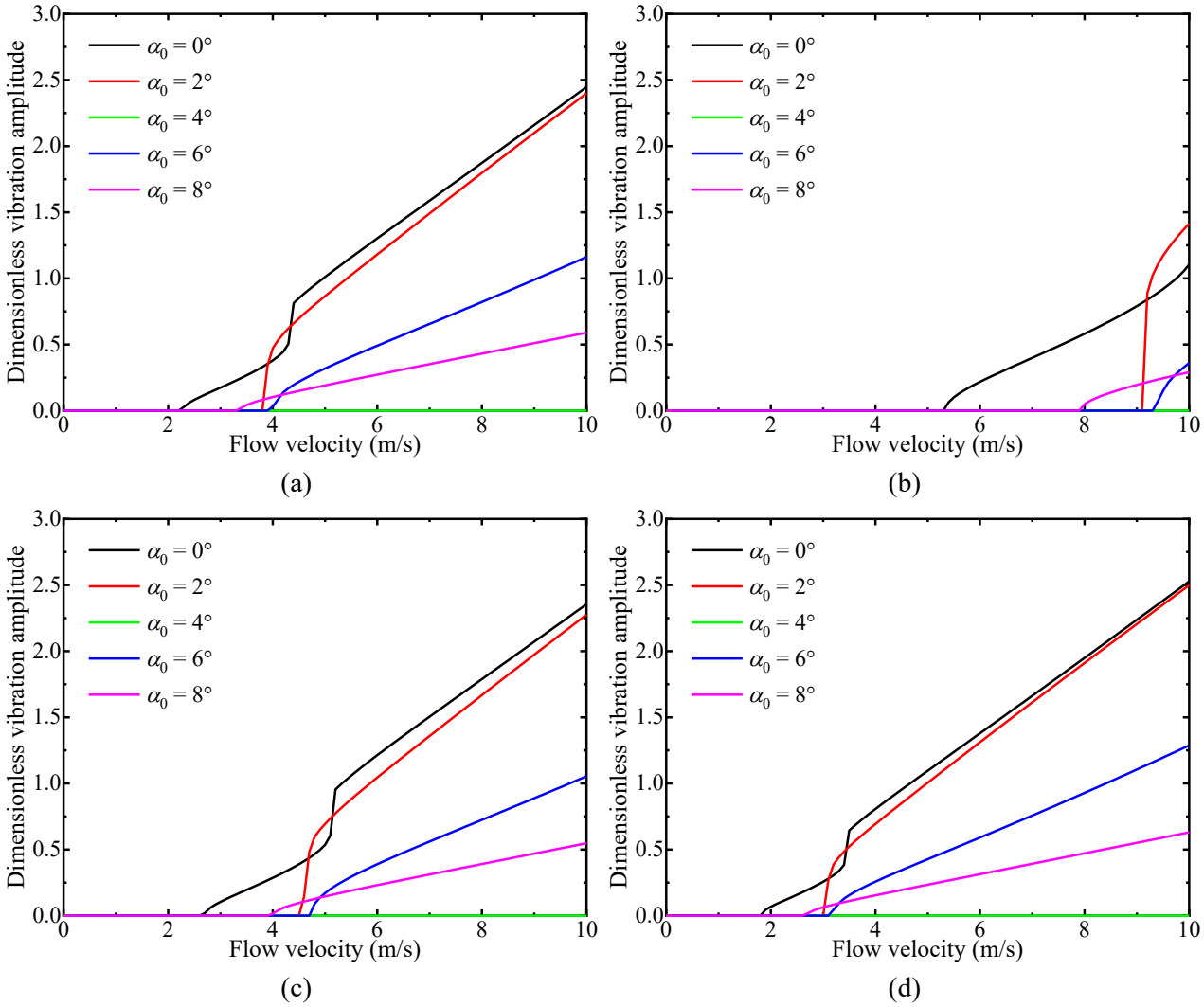

Figure 7. Displacement bifurcation diagrams for energy harvester with $r/d = 1/15$ cylinder at various predefined angles of attack and load resistances: (a) $R = 10^4$ Ω, (b) $R = 10^5$ Ω, (c) $R = 10^6$ Ω, and (d) $R = 10^7$ Ω.

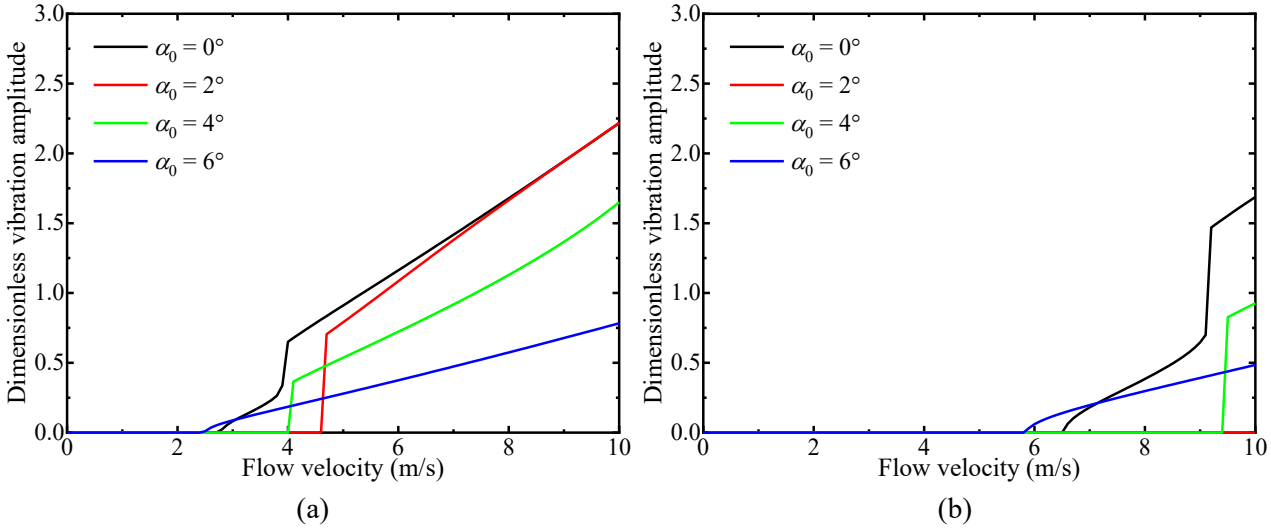

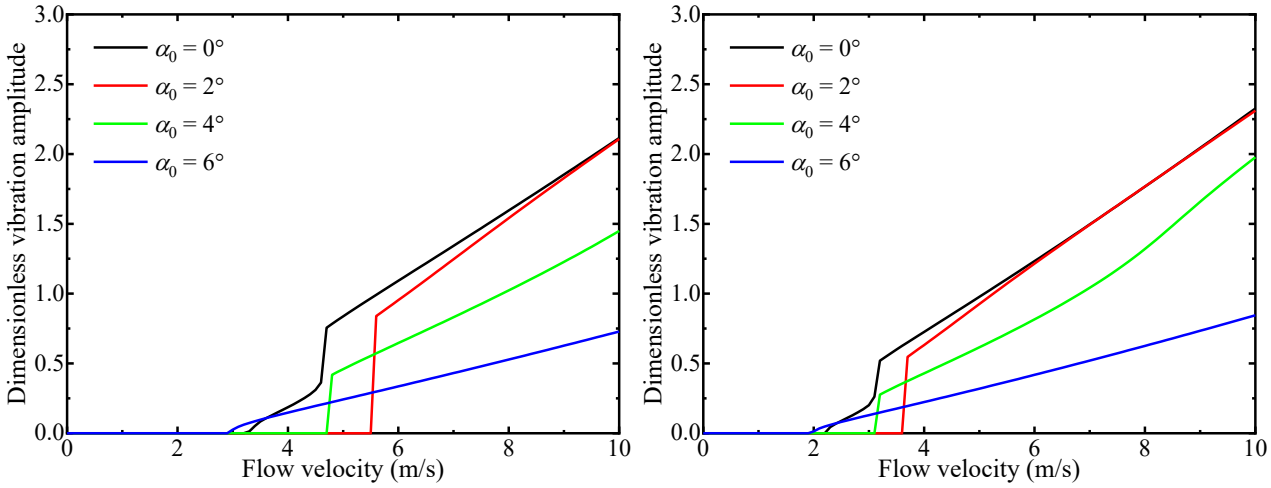

Figure 8. Displacement bifurcation diagrams for energy harvester with $r/d = 2/15$ cylinder at various predefined angles of attack and load resistances: (a) $R = 10^4$ Ω, (b) $R = 10^5$ Ω, (c) $R = 10^6$ Ω, and (d) $R = 10^7$ Ω.

To examine the effects of the predefined angle of attack and corner shape on the energy harvester's performance, Figures 9-11 show, respectively, the variation of power output versus flow velocity for the harvester with the sharp-edge cylinder, the cylinder with $r/d = 1/15$, and the cylinder with $r/d = 2/15$. The results show that the power outputs of all cylinders are largely affected by the predefined angle of attack. The considered energy harvesters yield the highest levels of power outputs around $R = 10^4$ or 10^6 Ω at relatively high flow velocities, which will be further studied later. The energy harvester with the sharp-edge cylinder is effective around $\alpha_0 = 0°$, 2°, 8°, and 10°, but it is ineffective around $\alpha_0 = 4°$ and 6°. The harvester with the $r/d = 1/15$ cylinder is effective around $\alpha_0 = 0°$, 2°, 6°, and 8°, but it is ineffective around $\alpha_0 = 4°$. Finally, the harvester with the $r/d = 2/15$ cylinder is effective within the range of $\alpha_0 = 0° \sim 6°$ but it is ineffective outside this range. It is also noted that the rounded corners slightly decrease the power outputs of the energy harvester.

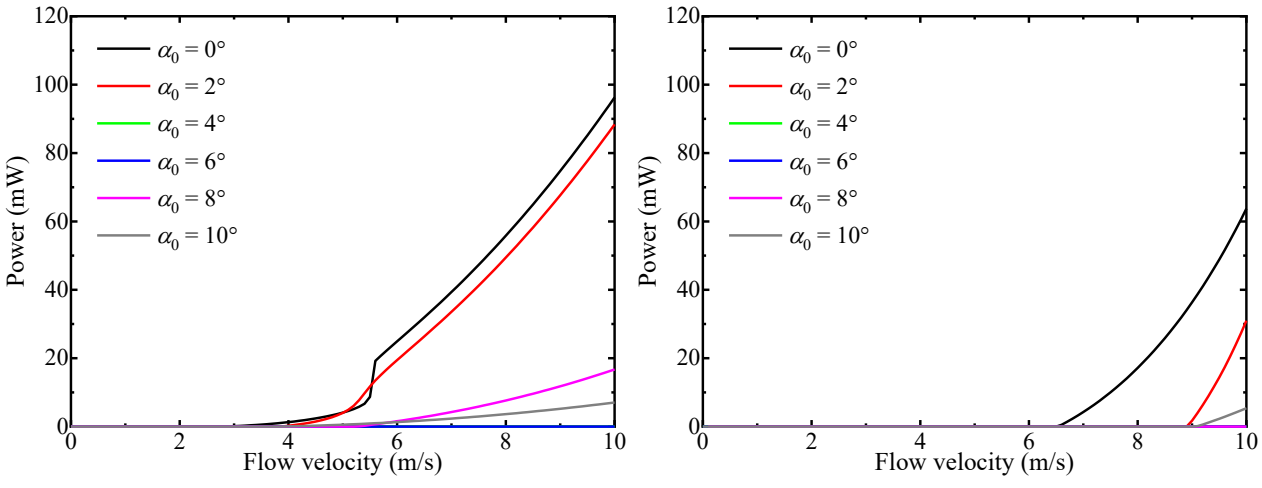

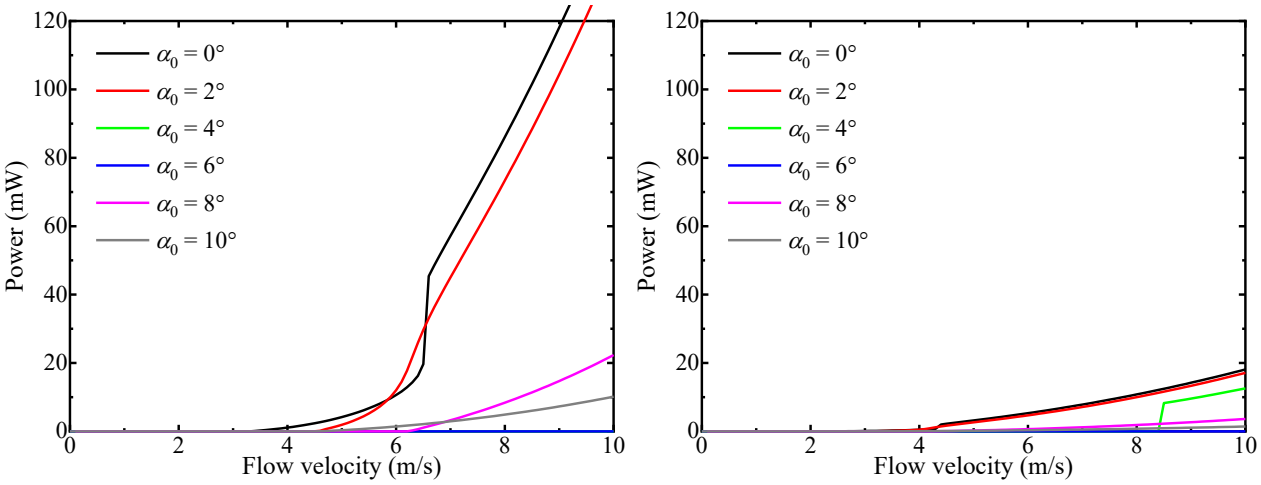

Figure 9. Power output bifurcation diagrams for of energy harvester with sharp-edge cylinder at various predefined angles of attack and load resistances: (a) $R = 10^4$ Ω, (b) $R = 10^5$ Ω, (c) $R = 10^6$ Ω, and (d) $R = 10^7$ Ω.

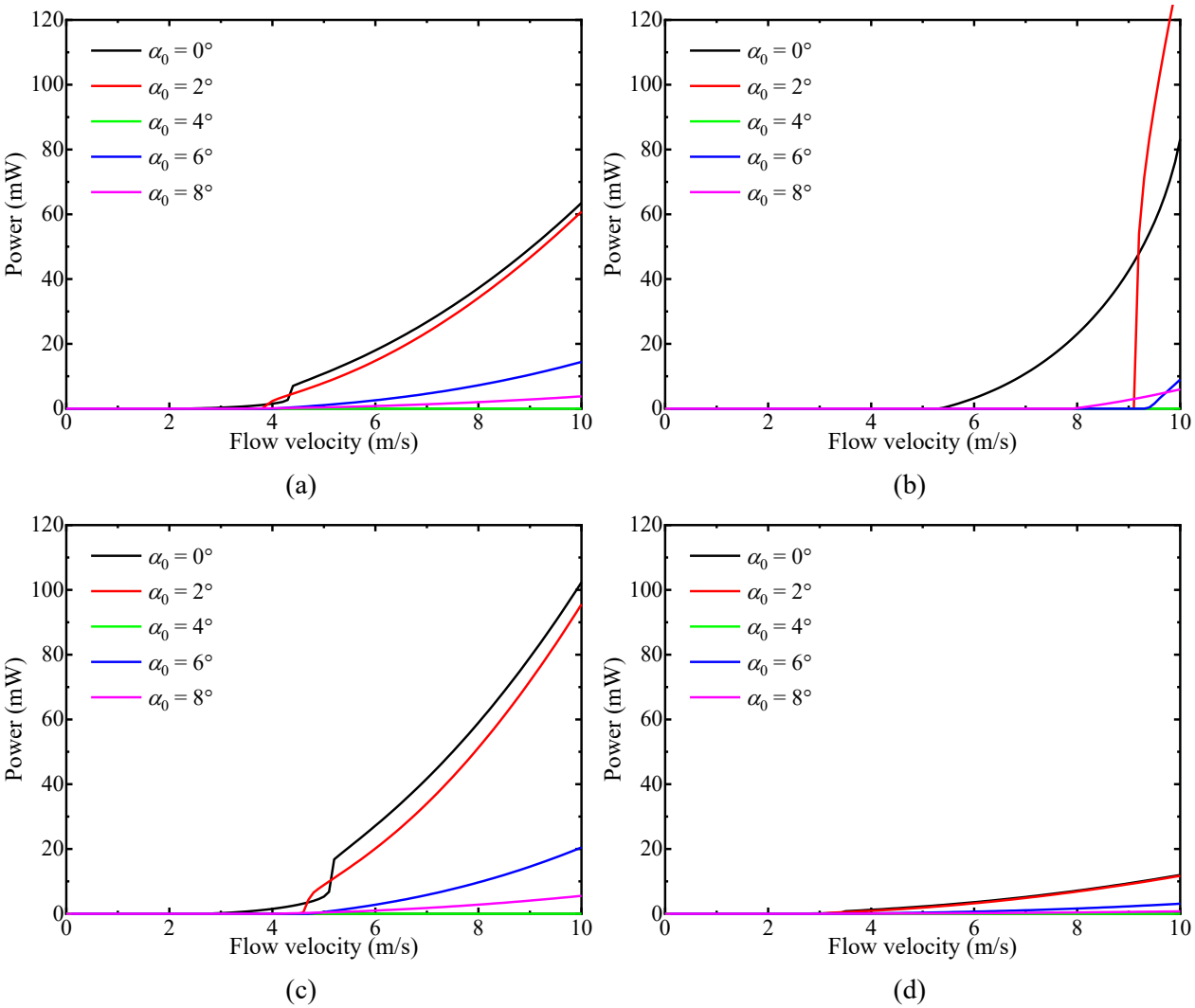

Figure 10. Power output bifurcation diagrams for energy harvester with $r/d = 1/15$ cylinder at various predefined angles of attack and load resistances: (a) $R = 10^4$ Ω, (b) $R = 10^5$ Ω, (c) $R = 10^6$ Ω, and (d) $R = 10^7$ Ω.

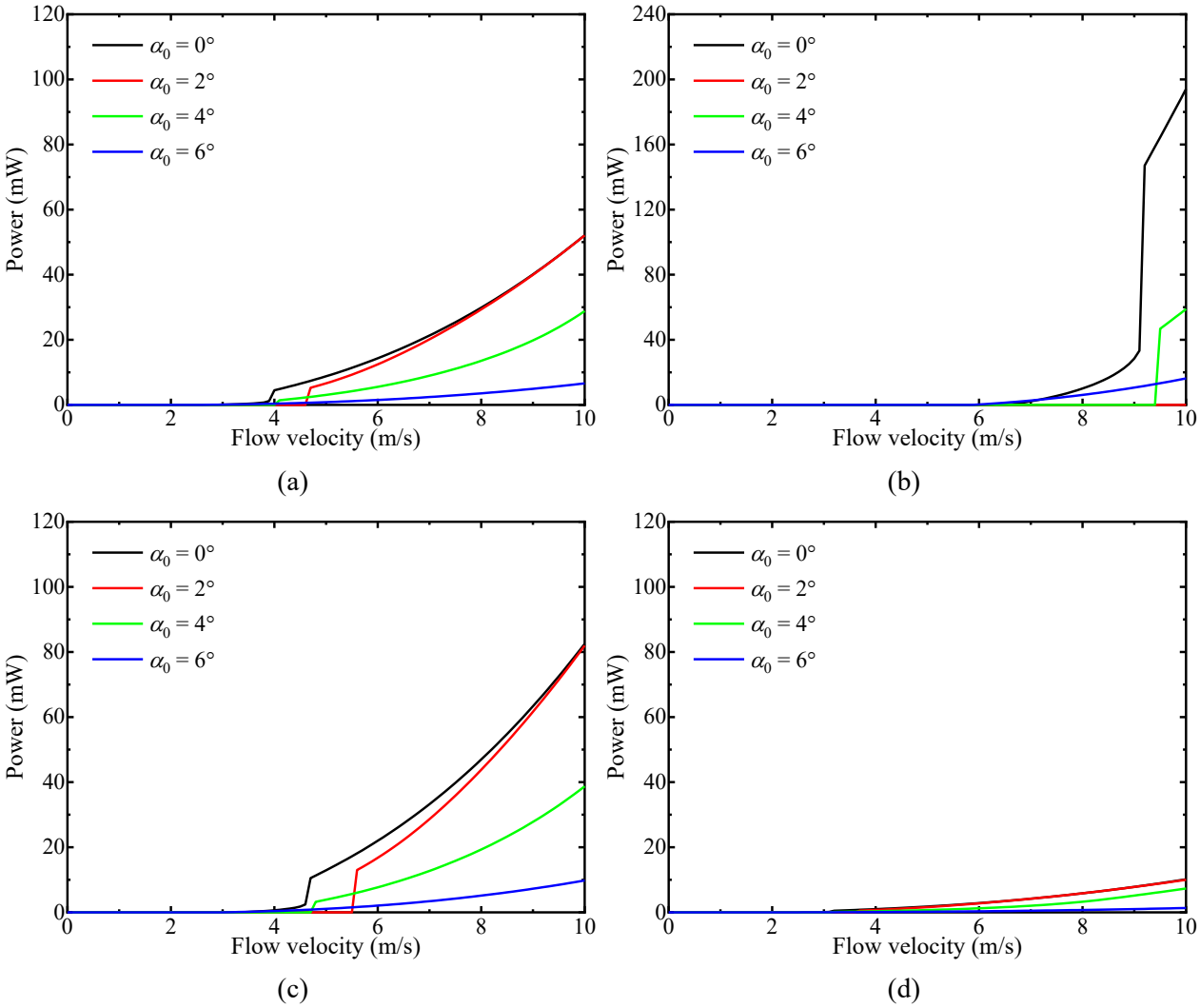

Figure 11. Power output bifurcation diagrams for energy harvester with $r/d = 2/15$ cylinder at various predefined angles of attack and load resistances: (a) $R = 10^4$ Ω, (b) $R = 10^5$ Ω, (c) $R = 10^6$ Ω, and (d) $R = 10^7$ Ω.

The vibrational displacement and power output of the fluid-structure-electrical system are then studied with varying electrical load resistances. Figure 12 presents the curves of the dimensionless vibration amplitudes versus the electrical load resistance for the harvesters with the sharp-edge cylinder, the cylinder with $r/d = 1/15$, and the cylinder with $r/d = 2/15$. The presented results correspond to a flow velocity of $U = 8$ m/s. It follows from Figure 12 that, with decreasing the electrical load resistance, the dimensionless vibration amplitudes first reduce and then enlarge for all bluff body configurations. The minimum vibration amplitudes are achieved around an electrical load resistance of $R = 10^5$ Ω. The observation is due to the largest piezoelectric coupling damping (and therefore larger onset galloping speed) around this value of load resistance. The transverse displacements for some cases are zero because the square cylinders for these cases do not gallop at $U = 8$ m/s.

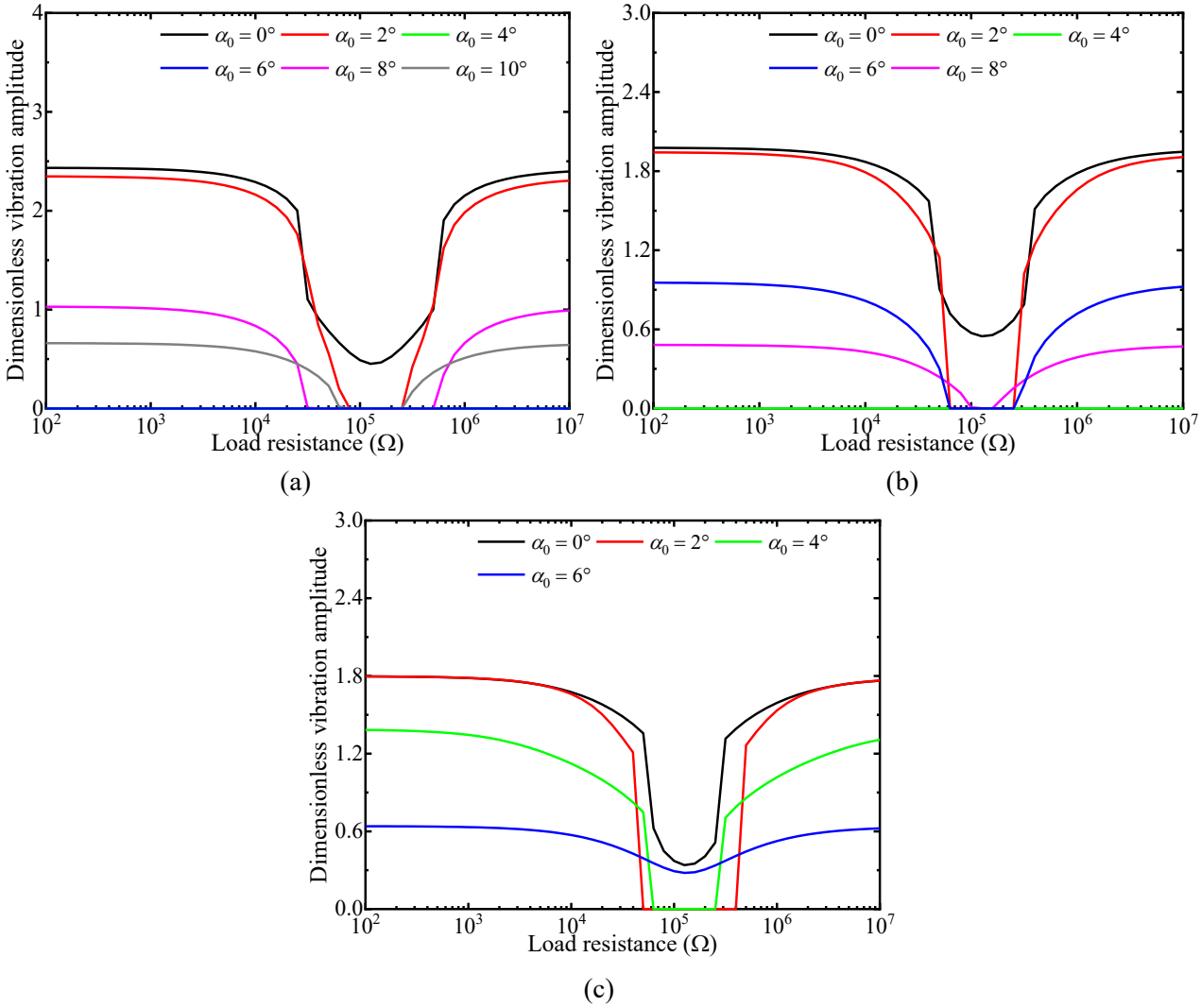

Figures 12. Variation of the transverse displacement versus the load resistance for harvester with (a) sharp-edge cylinder, (b) r/d = 1/15 cylinder, and (c) r/d = 2/15 cylinder.

Figure 13 shows curves of the power outputs versus the electrical load resistance for the energy harvesters with the sharp-edge cylinder, the cylinder with r/d = 1/15, and the cylinder with r/d = 2/15. The presented results correspond to a flow velocity of U = 8 m/s. Similar to the transverse displacements, the minimum power outputs are achieved approximately at a load resistance of $R = 10^5$ Ω. For each bluff body configuration, two optimum values of the electrical load resistances can be found where peak power outputs are achieved. It is also noted that the higher values of power outputs and sharp variations of the vibration amplitudes both occur in the load resistance ranges around $R = 10^5$ Ω. This result is very useful to enhance the performance of galloping-based piezoelectric energy harvesters with various bluff body configurations at different angles of attack. The results also show that the rounded corners reduce the harvested energy around $\alpha_0 = 0° \sim 2°$. However, the rounded corners enhance the robustness of the energy harvester by making its performance less sensitive to the angle of attack within $\alpha_0 = 0° \sim 6°$.

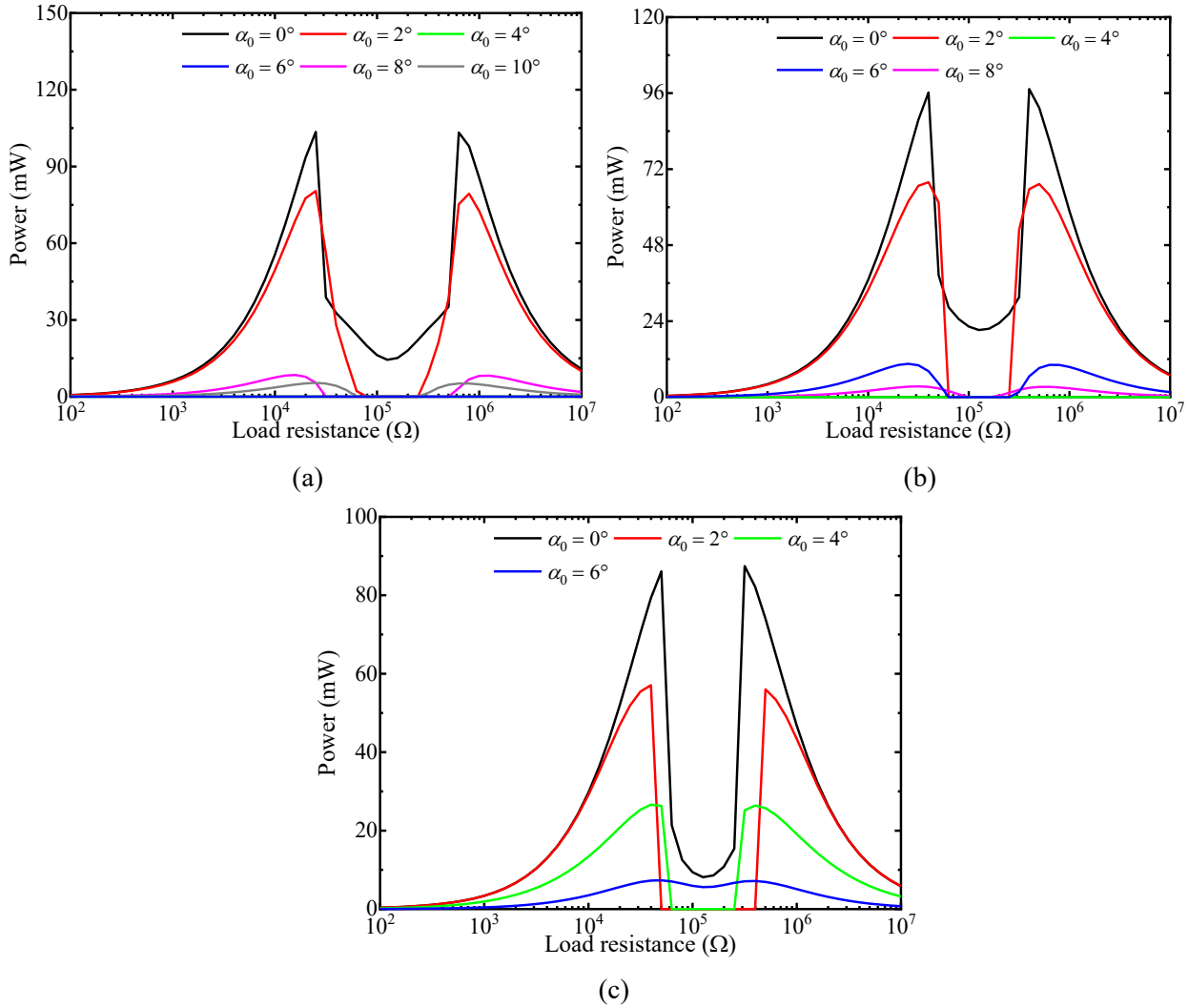

Figures 13. Variation of the power output versus the load resistance for harvester with (a) sharp-edge cylinder, (b) r/d = 1/15 cylinder, and (c) r/d = 2/15 cylinder.

5. Conclusions

This paper studied numerically the influences of the angle of attack and the corner shape on the effectiveness of square-shaped galloping energy harvesters. A piezoaeroelastic reduced-order modeling was considered when the galloping force is approximated based on the quasi-steady theory. Three bluff body configurations were considered, i.e., a sharp-edge square cylinder and two round-edge square cylinders with corner radii of r/d = 1/15 and 2/15, respectively. Numerical results proved that the onset wind speed of instability depends on the electrical load resistance while this dependency reduces as the natural frequency of the harvester becomes higher. For each bluff body configuration, the onset galloping velocity first increases with increasing the angle of attack and then decreases to a value close to that at $\alpha_0 = 0°$. In a range of small angles of attack ($\alpha_0 = 0° \sim 2°$), the onset velocities of the three configurations are very close. The rounded corners make the onset velocity less sensitive to the angle of attack. Additionally, all three cylinders exhibit the largest transverse displacements at the angle of attack $\alpha_0 = 0°$, while the displacements at $\alpha_0 = 2°$ are only

slightly lower than those at $\alpha_0 = 0°$. The effective α_0 range of the energy harvester is changed by the corner shapes. In general, the rounded corners slightly decrease the transverse displacements and power outputs of the energy harvesters. However, the rounded corners enhance the robustness of the energy harvester by making its performance less sensitive to the angle of attack within $\alpha_0 = 0° \sim 6°$. These conclusions are useful for choosing an appropriate corner shape or a predefined angle of attack for a practical energy harvester based on its surrounding flow condition.

Acknowledgments

This work was supported by the National Natural Science Foundation of China (Grant No.: 51977196), and China Postdoctoral Science Foundation (2020T130557).

References

1. Capel, I., Dorrell, H., Spencer, E., Davis, M., *The amelioration of the suffering associated with spinal cord injury with subperception transcranial electrical stimulation.* Spinal Cord, 2003. **41**(2): p. 109-117.
2. Muralt, P., *Ferroelectric thin films for micro-sensors and actuators: a review.* Journal of micromechanics and microengineering, 2000. **10**(2): p. 136.
3. Stephen, N.G., *On energy harvesting from ambient vibration.* Journal of sound and vibration, 2006. **293**(1-2): p. 409-425.
4. Adhikari, S., Friswell, M., Inman, D., *Piezoelectric energy harvesting from broadband random vibrations.* Smart Materials and Structures, 2009. **18**(11): p. 115005.
5. Zhao, L., Zou, H., Gao, Q., Yan, G., Wu, Z., Liu, F., Wei, K., Yang, B., Zhang, W., *Design, modeling and experimental investigation of a magnetically modulated rotational energy harvester for low frequency and irregular vibration.* Science China Technological Sciences, 2020. **63**: p. 2051-2062.
6. Chen, Z., Xia, Y., He, J., Xiong, Y., Wang, G., *Elastic-electro-mechanical modeling and analysis of piezoelectric metamaterial plate with a self-powered synchronized charge extraction circuit for vibration energy harvesting.* Mechanical Systems and Signal Processing, 2020. **143**: p. 106824.
7. Fan, K., Cai, M., Liu, H., Zhang, Y., *Capturing energy from ultra-low frequency vibrations and human motion through a monostable electromagnetic energy harvester.* Energy, 2019. **169**: p. 356-368.
8. Tao, K., Yi, H., Yang, Y., Chang, H., Wu, J., Tang, L., Yang, Z., Wang, N., Hu, L., Fu, Y., *Origami-inspired electret-based triboelectric generator for biomechanical and ocean wave energy harvesting.* Nano Energy, 2020. **67**: p. 104197.
9. Lai, Z., Wang, S., Zhu, L., Zhang, G., Wang, J., Yang, K., Yurchenko, D., *A hybrid piezo-dielectric wind energy harvester for high-performance vortex-induced vibration energy harvesting.* Mechanical Systems and Signal Processing. **150**: p. 107212.
10. Zhao, L.-C., Zou, H.-X., Yan, G., Liu, F.-R., Tan, T., Zhang, W.-M., Peng, Z.-K., Meng, G., *A water-proof magnetically coupled piezoelectric-electromagnetic hybrid wind energy harvester.* Applied Energy, 2019. **239**: p. 735-746.
11. Zhao, L.-C., Zou, H.-X., Yan, G., Liu, F.-R., Tan, T., Wei, K.-X., Zhang, W.-M., *Magnetic coupling and flextensional amplification mechanisms for high-robustness ambient wind energy harvesting.* Energy Conversion and Management, 2019. **201**: p. 112166.
12. Mehmood, A., Abdelkefi, A., Hajj, M., Nayfeh, A., Akhtar, I., Nuhait, A., *Piezoelectric energy harvesting from vortex-induced vibrations of circular cylinder.* Journal of Sound and Vibration, 2013. **332**(19): p. 4656-4667.

13. Wang, J., Geng, L., Ding, L., Zhu, H., Yurchenko, D., *The state-of-the-art review on energy harvesting from flow-induced vibrations.* Applied Energy, 2020. **267**: p. 114902.
14. Wang, J., Tang, L., Zhao, L., Zhang, Z., *Efficiency investigation on energy harvesting from airflows in HVAC system based on galloping of isosceles triangle sectioned bluff bodies.* Energy, 2019. **172**: p. 1066-1078.
15. Qin, W., Deng, W., Pan, J., Zhou, Z., Du, W., Zhu, P., *Harvesting wind energy with bi-stable snap-through excited by vortex-induced vibration and galloping.* Energy, 2019. **189**: p. 116237.
16. Sun, W., Jo, S., Seok, J., *Development of the optimal bluff body for wind energy harvesting using the synergetic effect of coupled vortex induced vibration and galloping phenomena.* International Journal of Mechanical Sciences, 2019. **156**: p. 435-445.
17. Wang, J., Gu, S., Zhang, C., Hu, G., Chen, G., Yang, K., Li, H., Lai, Y., Litak, G., Yurchenko, D., *Hybrid wind energy scavenging by coupling vortex-induced vibrations and galloping.* Energy Conversion and Management, 2020. **213**: p. 112835.
18. Zhang, M., Xu, F., Øiseth, O., *Aerodynamic damping models for vortex-induced vibration of a rectangular 4: 1 cylinder: Comparison of modeling schemes.* Journal of Wind Engineering and Industrial Aerodynamics, 2020. **205**: p. 104321.
19. Zhang, M., Xu, F., Yu, H., *A simplified model to evaluate peak amplitude for vertical vortex-induced vibration of bridge decks.* International Journal of Mechanical Sciences. **192**: p. 106145.
20. Abdelkefi, A., Hajj, M.R., Nayfeh, A.H., *Power harvesting from transverse galloping of square cylinder.* Nonlinear Dynamics, 2012. **70**(2): p. 1355-1363.
21. Yang, K., Qiu, T., Wang, J., Tang, L., *Magnet-induced monostable nonlinearity for improving the VIV-galloping-coupled wind energy harvesting using combined cross-sectioned bluff body.* Smart Materials and Structures, 2020. **29**(7): p. 07LT01.
22. Yang, Y., Zhao, L., Tang, L., *Comparative study of tip cross-sections for efficient galloping energy harvesting.* Applied Physics Letters, 2013. **102**(6): p. 064105.
23. Wang, Q., Zou, H.-X., Zhao, L.-C., Li, M., Wei, K.-X., Huang, L.-P., Zhang, W.-M., *A synergetic hybrid mechanism of piezoelectric and triboelectric for galloping wind energy harvesting.* Applied Physics Letters, 2020. **117**(4): p. 043902.
24. Bryant, M., Garcia, E., *Modeling and testing of a novel aeroelastic flutter energy harvester.* Journal of vibration and acoustics, 2011. **133**(1).
25. Zhang, M., Xu, F., Zhang, Z., Ying, X., *Energy budget analysis and engineering modeling of post-flutter limit cycle oscillation of a bridge deck.* Journal of Wind Engineering and Industrial Aerodynamics, 2019. **188**: p. 410-420.
26. Zhang, M., Xu, F., Ying, X., *Experimental investigations on the nonlinear torsional flutter of a bridge deck.* Journal of Bridge Engineering, 2017. **22**(8): p. 04017048.
27. Zou, H.-X., Zhao, L.-C., Gao, Q.-H., Zuo, L., Liu, F.-R., Tan, T., Wei, K.-X., Zhang, W.-M., *Mechanical modulations for enhancing energy harvesting: Principles, methods and applications.* Applied Energy, 2019. **255**: p. 113871.
28. Den Hartog, J.P., *Mechanical vibrations*. 1985: Courier Corporation.
29. Parkinson, G., Smith, J., *The square prism as an aeroelastic non-linear oscillator.* The Quarterly Journal of Mechanics and Applied Mathematics, 1964. **17**(2): p. 225-239.
30. Parkinson, G., Brooks, N., *On the aeroelastic instability of bluff cylinders.* 1961.
31. Barrero-Gil, A., Alonso, G., Sanz-Andres, A., *Energy harvesting from transverse galloping.* Journal of Sound and Vibration, 2010. **329**(14): p. 2873-2883.
32. Javed, U., Abdelkefi, A., *Role of the galloping force and moment of inertia of inclined square cylinders on the performance of hybrid galloping energy harvesters.* Applied Energy, 2018. **231**: p. 259-276.
33. Abdelkefi, A., Yan, Z., Hajj, M.R., *Performance analysis of galloping-based piezoaeroelastic energy harvesters*

with different cross-section geometries. Journal of Intelligent Material Systems and Structures, 2014. **25**(2): p. 246-256.

34. Abdelkefi, A., Yan, Z., Hajj, M.R., *Modeling and nonlinear analysis of piezoelectric energy harvesting from transverse galloping.* Smart materials and Structures, 2013. **22**(2): p. 025016.
35. Javed, U., Abdelkefi, A., *Impacts of the aerodynamic force representation on the stability and performance of a galloping-based energy harvester.* Journal of Sound and Vibration, 2017. **400**: p. 213-226.
36. Zhang, B., Mao, Z., Song, B., Ding, W., Tian, W., *Numerical investigation on effect of damping-ratio and mass-ratio on energy harnessing of a square cylinder in FIM.* Energy, 2018. **144**: p. 218-231.
37. Nemes, A., Zhao, J., Jacono, D.L., Sheridan, J., *The interaction between flow-induced vibration mechanisms of a square cylinder with varying angles of attack.* 2012.
38. Zhao, J., Leontini, J.S., Jacono, D.L., Sheridan, J., *Fluid–structure interaction of a square cylinder at different angles of attack.* Journal of Fluid Mechanics, 2014. **747**: p. 688-721.
39. Tang, Z., Zhou, B., *The effect of mass ratio and spring stiffness on flow-induced vibration of a square cylinder at different incidence angles.* Ocean Engineering, 2020. **198**: p. 106975.
40. Zhang, M., Xu, F., Han, Y., *Assessment of wind-induced nonlinear post-critical performance of bridge decks.* Journal of Wind Engineering and Industrial Aerodynamics, 2020. **203**: p. 104251.
41. Tamura, T., Miyagi, T., *The effect of turbulence on aerodynamic forces on a square cylinder with various corner shapes.* Journal of Wind Engineering and Industrial Aerodynamics, 1999. **83**(1-3): p. 135-145.
42. Carassale, L., Freda, A., Marre-Brunenghi, M., *Effects of free-stream turbulence and corner shape on the galloping instability of square cylinders.* Journal of Wind Engineering and Industrial Aerodynamics, 2013. **123**: p. 274-280.
43. Parkinson, G., Wawzonek, M., *Some considerations of combined effects of galloping and vortex resonance.* Journal of Wind Engineering and Industrial Aerodynamics, 1981. **8**(1-2): p. 135-143.
44. Laneville, A., *Effects of turbulence on wind induced vibrations of bluff cylinders*. 1973, University of British Columbia.
45. Yang, X., He, X., Li, J., Jiang, S., *Modeling and verification of piezoelectric wind energy harvesters enhanced by interaction between vortex-induced vibration and galloping.* Smart Materials and Structures, 2019. **28**(11): p. 115027.
46. Abdelkefi, A., Hajj, M., Nayfeh, A., *Piezoelectric energy harvesting from transverse galloping of bluff bodies.* Smart Materials and Structures, 2012. **22**(1): p. 015014.
47. Yu, H., Zhang, M., *Effects of side ratio on energy harvesting from transverse galloping of a rectangular cylinder.* Energy, 2021. **226**: p. 120420.